Journal of Magnetic Resonance **148,** 135–141 (2001)
doi:10.1006/jmre.2000.2215, available online at http://www.idealibrary.com on IDEAL®

Radial-Field Sidebands in MAS

Piotr Tekely* and Maurice Goldman†

**Laboratoire de Méthodologie RMN, UPRESA CNRS 7042, Université H. Poincaré, Nancy I, 54506 Vandoeuvre-lès-Nancy, France; and †CEA/DRECAM, Service de Physique de l'Etat Condensé, CEA Saclay, 91191 Gif sur Yvette, France*

Received June 26, 2000; revised September 12, 2000

The existence of sidebands at $\pm\nu_r$ in MAS spectra due to the radial component of the RF field at the edges of the coil is described theoretically and illustrated experimentally. The height of the radial-field sidebands does not depend on the spinning speed and may contribute significantly to the intensity of -1 spinning sideband of MAS modulated internal interactions for a sample placed in a rotor of length exceeding the solenoid coil or a small volume sample placed at the edge of the coil.

Key Words: **radial RF field; spinning sidebands; MAS.**

INTRODUCTION

The effect of a shift of the NMR resonance frequency induced by sample spinning when the RF field is radial has been described theoretically and illustrated experimentally in a previous article (*1*) (henceforth I). The main emphasis of this previous work considered the case when the RF field amplitude was constant, resulting in a single frequency shift equal to the spinning frequency. This paper did note the spinning sidebands generation when this amplitude is not constant, such as in magic-angle spinning. This was very schematic, incomplete, and not entirely correct. However, the experimental observation of a similar effect, with certain characteristics in apparent contradiction with the suggestion of (I), has prompted us to perform a more thorough theoretical analysis of this case.

The aim of this article is threefold. First, any new effect, suggested by either theory or experiment, is worthy of investigation. Second, the use of MAS is so widespread that an observation of experimental features for which no clean description is available in the literature is likely to be puzzling or, worse, misleading. Last but not least, the analysis of spinning sideband (ssb) manifolds resulting from rotation-induced coherent modulation of internal interactions such as chemical shift anisotropy and dipolar and quadrupolar interactions is now routinely exploited to extract the structural and motional information through the principal values of corresponding tensors and their mutual orientations (*2*). When exploiting this information from the ssb manifold it is therefore important to be aware of possible experimental and instrumental artifacts affecting the intensity of individual spinning sidebands relating to the internal interactions.

We begin by briefly recalling the basis of the theory developed in (I). This is followed with an analysis of the radial-field effect when spinning around the magic-angle axis and then is illustrated with the experimental results.

THEORETICAL FRAMEWORK AND BASIC EQUATIONS

The starting point of the theory in (I) is the reciprocity principle (*1, 3, 4*): the emf induced in a coil by a magnetization distribution $\mathbf{m}(\mathbf{r})$ is equal to

$$V = -\frac{d}{dt}\int \mathbf{B}_1(\mathbf{r})\cdot\mathbf{m}(\mathbf{r})d^3r, \qquad [1]$$

where $\mathbf{B}_1(\mathbf{r})$ is the field produced at point $\mathbf{r}$ by a current of unit intensity in the coil. In NMR, the field $\mathbf{B}_1$ and the magnetization $\mathbf{m}$ are limited to their part perpendicular to the direction Oz of the external steady magnetic field B_0, and the magnetization is precessing at the Larmor frequency ω_0. It is convenient to use semi-polar coordinates and to express all vectors in the xy plane in the form of complex numbers, i.e.,

$$\begin{cases}\mathbf{B}_1(\rho, z, \theta) \rightarrow B_1(\rho, z, \theta)\\ \mathbf{m}(\rho, z, \theta) \rightarrow m(\rho, z, \theta),\end{cases} \qquad [2]$$

whence

$$\mathbf{B}_1\cdot\mathbf{m} = \tfrac{1}{2}(B_1m^* + B_1^*m) = \mathrm{Re}(B_1^*m). \qquad [3]$$

Following the usage in NMR, we keep the magnetization in the form of a complex number m, and we use

$$\mathbf{B}_1\cdot\mathbf{m} = B_1^*m. \qquad [4]$$

Neglecting relaxation, for a static sample the evolution of the magnetization following a RF pulse is

$$m(\rho, z, \theta; t) = m(\rho, z, \theta; 0)\exp(i\omega_0 t). \qquad [5]$$

It is initially locally normal to the pulse RF field, that is

1090-7807/01 $35.00

imaginary. The case essentially studied in (I) is that when the coil axis is parallel to Oz, in which case the amplitudes of both B_1 and m are constant and radial. They are written

$$\begin{cases} B_1(\rho, z, \theta) = b_1(\rho, z)\exp(i\theta) \\ m(\rho, z, \theta; 0) = ia(\rho, z)\exp(i\theta). \end{cases} \quad [6]$$

For such a static sample, the emf takes the form

$$V = 2\pi\omega_0\exp(i\omega_0 t)\int\int \rho d\rho\, dz\, b_1^*(\rho, z)a(\rho, z). \quad [7]$$

In the case when the sample is rotating at frequency Ω, the sample element located at position (ρ, z, θ) at time t is that which was initially at position $[\rho, z, (\theta - \Omega t)]$, that is,

$$\begin{aligned} m(\rho, z, \theta; t) &= m[\rho, z, (\theta - \Omega t); 0]\exp(i\omega_0 t) \\ &= ia(\rho, z)\exp[i(\theta - \Omega t)]\exp(i\omega_0 t), \end{aligned} \quad [8]$$

and one obtains in place of Eq. [7]

$$V = 2\pi\omega_0\exp[i(\omega_0 - \Omega)t]\int\int \rho d\rho\, dz\, b_1^*(\rho, z)a(\rho, z), \quad [9]$$

that is a frequency shift algebraically equal to $-\Omega$ and a signal amplitude independent of the spinning frequency. This is the basic result of article (I).

Magic-Angle Spinning

MAS consists of using a sample spinning around an axis oriented in a direction OZ forming the "magic" angle $\beta = \arccos(1/\sqrt{3})$ with the direction Oz of the external field. As a general rule, the coil is axially symmetric around the axis OZ (Fig. 1a). The RF field it produces is aligned with this axis, as a rule, except near the edges of the coil, where it acquires a radial component. In the system of axes OXYZ associated with the coil, the coordinates of a given point can be expressed in cylindrical coordinates Z, ρ, θ with $X = \rho\cos\theta$ and $Y = \rho\sin\theta$. Due to the symmetry of the coil around the axis OZ, for all points of equal components Z and ρ, the amplitude of the radial component is independent of the polar angle θ in the XY plane perpendicular to the spinning axis OZ. However, it is only the component of the RF field in the xy plane normal to the external field direction Oz which is able to induce transitions, that is which is active for rotating the spins during a pulse and also for representing the "unit current" to be used in the reciprocity theorem. We must therefore consider only the projection of the RF field on that plane. This is schematically shown in Fig. 1b with the superposition of two planes. The solid circle represents the constant amplitude of the radial-field

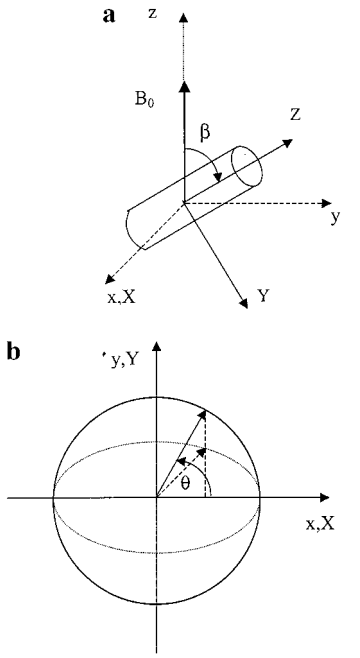

FIG. 1. The frames of reference used in the text. (a) The lab frame xyz is related to the rotor frame XYZ. Near the coil edges, the RF field has radial components with respect to OZ. (b) The radial component of the RF field in the plane XY (solid circle) and its projection in the plane xy (dashed ellipse). As an illustration for a given angle θ in the XY plane, the radial field and its projection correspond to the solid and dashed arrows, respectively.

component in the plane XY as a function of the angle θ and the dashed ellipse represents its projection in the plane xy: it has no longer a constant amplitude as a function of the polar angle θ. For a purely radial RF field this has a double consequence. First, during the pulse prior to the observation of the FID, the angle α by which the spins are tilted will depend on the polar angle θ, so that the initial magnetization, proportional to $\sin\alpha$, will also depend on θ. Second, the amplitude b_1 entering the expression of the emf depends also on that angle θ. Therefore, Eq. [6] is now to be replaced by

$$\begin{cases} B_1(\rho, Z, \theta) = b_1(\rho, Z, \theta)\exp(i\theta) \\ m(\rho, Z, \theta) = ia(\rho, Z, \theta)\exp(i\theta), \end{cases} \quad [10]$$

where b_1 and a are real: it is their amplitude which changes, not their orientation. In the case when the RF field has a component of constant orientation along OZ, its projection normal to the main field axis Oz is along the axis Oy. We treat in turn the case when the RF field is purely radial and then the general case when the component of constant orientation does not vanish.

(a) Purely radial RF field. As above, we "isolate" a ring of constant Z and ρ. For this ring, the RF field components normal to Oz are easily derived from Fig. 1:

$$\begin{cases} B_{1x} = b\ \cos\ \theta \\ B_{1y} = b\ \cos\ \beta\ \sin\ \theta = b\ \sin\ \theta/\sqrt{3}, \end{cases} \quad [11]$$

where b is related to the amplitude b_1 by

$$b_1 = b\sqrt{\cos^2\theta + \sin^2\theta/3}. \quad [12]$$

The complex notation for the field then reads

$$B_1(\theta) = b[p\ \exp(i\theta) + q\ \exp(-i\theta)];$$
$$p = \tfrac{1}{2}(1 + 1/\sqrt{3}); \quad q = \tfrac{1}{2}(1 - 1/\sqrt{3}). \quad [13]$$

The initial transverse magnetization is proportional to the sine of the local pulse angle (and locally in quadrature with the RF field), and, to within a constant, it is equal to

$$m(\theta) = \frac{\sin[\lambda b_1(\theta)]}{b_1(\theta)} \times [p\ \exp(i\theta) + q\ \exp(-i\theta)], \quad [14]$$

where $\lambda b_1(\theta)$ is the local pulse angle. Since during the pulse the RF field, although very different from $b_1(\theta)$, is proportional to it, λ is a constant proportional to the pulse duration. As for

$$[p\ \exp(i\theta) + q\ \exp(-i\theta)]/b_1(\theta),$$

it describes a vector parallel to $B_1(\theta)$ and of modulus $1/b$ independent of θ.

The contribution of the ring to the emf is of the form

$$dV = \omega_0 \exp(i\omega_0 t)\rho d\rho\ dz \int_0^{2\pi} B_1^*(\theta) m(\theta - \Omega t) d\theta. \quad [15]$$

This form is adequate for small pulse angles, for which $\sin(\lambda b_1)/b_1$ reduces to λ. For an arbitrary pulse angle, it proves much more convenient to use an equivalent expression,

$$dV = \omega_0 \exp(i\omega_0 t)\rho d\rho\ dz \int_0^{2\pi} B_1^*(\theta + \Omega t) m(\theta) d\theta. \quad [16]$$

With the help of Eqs. [13] and [14], we obtain

$$dV = \omega_0 \exp(i\omega_0 t)\rho d\rho\ dz \times \{A(-\Omega)\exp(-i\Omega t) + A(\Omega)\exp(i\Omega t)\} \quad [17]$$

with

$$A(-\Omega) = \int_0^{2\pi} \zeta(\theta)(p^2 + pq\ \exp(-2i\theta)) d\theta$$

$$A(\Omega) = \int_0^{2\pi} \zeta(\theta)(q^2 + pq\ \exp(2i\theta)) d\theta$$

$$\zeta(\theta) = \sin(\lambda b_1)/b_1. \quad [18]$$

In the linear limit, when $\lambda b_1 \ll 1$, the factor $\zeta(\theta)$ reduces to the θ-independent value λ, so that the integrals of the exponential factors vanish, and the sideband amplitudes reduce to

$$A(-\Omega) = 2\pi\lambda p^2;\ A(\Omega) = 2\pi\lambda q^2 \quad [19]$$

and their ratio is then

$$A(-\Omega)/A(\Omega) = p^2/q^2 \approx 14, \quad [20]$$

a result which corrects that given in article (I).

It can be shown in full generality that the amplitudes are real. Indeed, the imaginary part of $A(\Omega)$ equals

$$\mathrm{Im}[A(\Omega)] = \int_0^{2\pi} (\sin(\lambda b_1)/b_1)(pq\ \sin(2\theta)) d\theta$$
$$= 2pq \int_0^{2\pi} \frac{\sin(\lambda b \sqrt{1 - 2\ \sin^2\theta/3})}{b\sqrt{1 - 2\ \sin^2\theta/3}} \times \sin\ \theta\ \cos\ \theta d\theta, \quad [21]$$

which can be decomposed into an integral from $-\pi/2$ to $\pi/2$ plus one from $\pi/2$ to $3\pi/2$. Writing $\sin\ \theta = u$, we have $\cos\ \theta d\theta = du$ and

$$\mathrm{Im}[A(\Omega)] = \int_{-1}^{+1} f(u) du + \int_{+1}^{-1} f(u) du = 0. \quad [22]$$

The same result is obtained for $A(-\Omega)$.

In order to compare the phase of sidebands with that of the normal, unshifted signal, we may remark that the latter, originating from the constant orientation of the RF field, corresponds to the absence of a dependence on the phase angle θ, and it gives rise to a real coefficient of $\exp(i\omega_0 t)$ for the emf it produces. As a consequence, if the Fourier transform of the FID is phased so as to display the normal unshifted signal in absorption, then the sidebands are also in pure absorption.

(b) The general case. We now include a component of constant orientation along the axis Oy. In place of Eq. [11], the field components are written under the form

$$\begin{cases} B_{1x} = b \cos\theta \\ B_{1y} = b(\sin\theta/\sqrt{3} + d), \end{cases} \quad [23]$$

where the constant-orientation component is equal to bd, so that d is a dimensionless parameter. This results in a slight simplification of the next equation. The amplitude b_1 is now equal to

$$b_1 = b\sqrt{\cos^2\theta + (\sin\theta/\sqrt{3} + d)^2}, \quad [24]$$

from which we obtain the expression for $B_1^*(\theta + \Omega t)$:

$$B_1^*(\theta + \Omega t) = b\{p \exp[-i(\theta + \Omega t)] + q \exp[i(\theta + \Omega t)] - id/2\}, \quad [25]$$

which yields for the sidebands an expression of the same form as Eq. [17], with

$$A(-\Omega) = \int_0^{2\pi\pi} \zeta(\theta)(p^2 + pq \exp(-2i\theta) + \tfrac{1}{2} idp \exp(-i\theta))d\theta$$

$$A(\Omega) = \int_0^{2\pi} \zeta(\theta)(q^2 + pq \exp(2i\theta) + \tfrac{1}{2} idq \exp(i\theta))d\theta, \quad [26]$$

where $\zeta(\theta)$ has the same form as in Eq. [18], with b_1 given by Eq. [24].

As for the case of a purely radial field, these amplitudes are real, that is they correspond to absorption signals when the central signal is in absorption. It is sufficient to prove it for, say, $A(\Omega)$. We have

$$\mathrm{Im}[A(\Omega)] = \int_0^{2\pi} \zeta(\theta)(pq \sin(2\theta) + \tfrac{1}{2} qd \cos\theta)d\theta$$

$$= q\int_0^{2\pi} \frac{\sin(\lambda b\sqrt{1 - \sin^2\theta + (\sin\theta/\sqrt{3} + d)^2})}{b\sqrt{1 - \sin^2\theta + (\sin\theta/\sqrt{3} + d)^2}} \times (2p \sin\theta + d)\cos\theta d\theta \quad [27]$$

and, by writing $\sin\theta = u$, we obtain an expression of the same form as Eq. [22], which proves the statement.

(c) Remarks and comments. The following comments can be made in connection with the above theory.

(1) In all cases, the amplitudes of the sidebands are predicted to be independent of the spinning frequency, in complete contrast with the sidebands originating from a modulation of the anisotropic interactions like chemical shifts or quadrupole couplings. This provides a decisive test as to the origin of the observed sidebands.

(2) The form of $m \propto \lambda b_1$ is a complicated function of θ (see Eqs. [12] and [24]), whose Fourier transform contains many harmonics. This is to be contrasted with the simplicity of the form of $B_1(\theta)$ (Eqs. [13] and [23]). Indeed, except in the limit of very small pulse angles, the form [16] is much easier to use than [15], since it shifts the dependence on Ωt from m to B_1. This makes it immediately visible that there are only two sidebands, at $+\Omega$ and $-\Omega$.

(3) From a practical point of view, the radial-field and the constant-orientation amplitudes vary continuously within the sample, and the observed sidebands correspond to an integral of Eqs. [26] over a continuum of values of b, d, and λ, whose weights would require an elaborate computation. We did not attempt such a computation in the experiments to be described. The case of a loosely packed powder sample is even more complicated, since the powder may move toward the external part of the sample tube under the effect of the centrifugal force during sample spinning, so that the exact sample distribution is not known with accuracy. The most important qualitative feature of the theory is that the relative amplitudes of the two sidebands depend in a complicated fashion on the coil and sample geometries and on the pulse length. It may be noted that the effect described in this article is not the only source of parasitic sidebands. Indeed, it was noticed very early that in liquids the inhomogeneity of intensity of either the main field B_0 or the radiofrequency field B_1 is responsible for sidebands in the spinning samples used for producing a line narrowing (*5–7*), an observation extended to the case when the orientation of the RF field is position-dependent (*8*). Similar and more complex effects were also detected and analyzed in rotary resonance recoupling experiments (*9*).

EXPERIMENTAL VERIFICATIONS

The presence of radial-field sidebands may be easily observed in high-resolution MAS spectra with narrow resonance signals on a standard probe using a sample in a rotor of length exceeding the solenoid coil. This is illustrated in Fig. 2, which shows three standard cross-polarization MAS spectra of adamantane recorded at three different spinning frequencies. These spectra clearly show the presence of $\pm\nu_r$ sidebands and the absence of any second- or higher-order sidebands. These features cannot be related to a residual chemical shift anisotropy of adamantane molecules which, at room temperature, rotate nearly isotropically. Clearly, no second-rank tensor in-

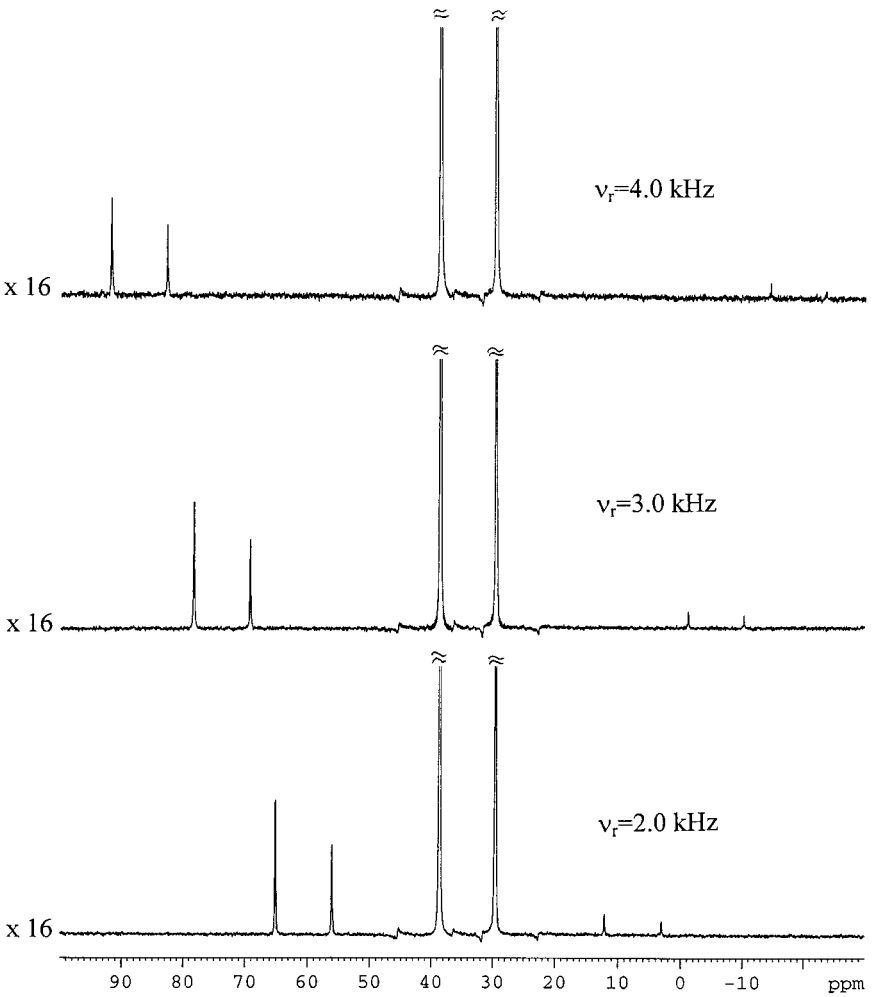

FIG. 2. Radial-field sidebands in the ^{13}C CP/MAS spectra of adamantane recorded at three different spinning frequencies by using a standard BRUKER probe. A sample is contained in the Φ7-mm rotor with length of 18 mm largely exceeding the solenoid coil (seven turns, Φ, and length of 9 mm). For better visualization, each spectrum is presented with a 16-fold increase of the amplitude.

teraction could be responsible for the appearance of $\pm\nu_r$ sidebands. Indeed, according to the theoretical treatment presented above, the observed $\pm\nu_r$ sidebands have to be produced by the radial part of the RF field at the edges of the solenoid coil. To check this hypothesis, we have compared the spectra of adamantane for a loosely packed sample with those recorded for a small volume sample placed at different heights in the rotor. Figure 3 shows such spectra at two spinning speeds. Compared with spectra recorded for the loosely packed sample, practically a complete disappearing and dramatic increase of the -1 sideband is observed for a 3-mm slice of adamantane placed in the central part and at the bottom of the rotor, respectively. This proves that the radial component of the RF field is responsible for the presence of the observed ± 1 sidebands. The similar effect of a huge increase of the intensity of radial-field induced sidebands can be observed for a sample placed at the top of the rotor, the single pulse spectra instead of cross-polarization transfer showing the same characteristics. For these "edge" positions of the sample, the ratio of intensity of sidebands $I^{(-1)}/I^{(+1)}$ at spinning frequency of 1 kHz is close to 12, which is in good agreement with the theoretical ratio (vide supra).

As expected, besides a largely dominating -1 sideband, another unusual feature of radial-field sidebands is their constant amplitude at different spinning speeds. This fact can be observed for small volume samples placed at the edge of coil and tightly packed to avoid the displacement of powder at higher spinning speeds. This is illustrated in Fig. 4, which shows a series of standard one-pulse spectra of benzene-solvated C_{60} with approximately constant intensity at higher spinning speeds of the -1 "purely radial-field" sideband of the C_{60} signal. Due to the fact that no second-rank tensor governs the radial-field sidebands, they may also manifest themselves when using the techniques of suppression of spinning sidebands. Indeed, as shown in Fig. 5, the TOSS pulse sequence is able to suppress efficiently the ssb resulting from the MAS-

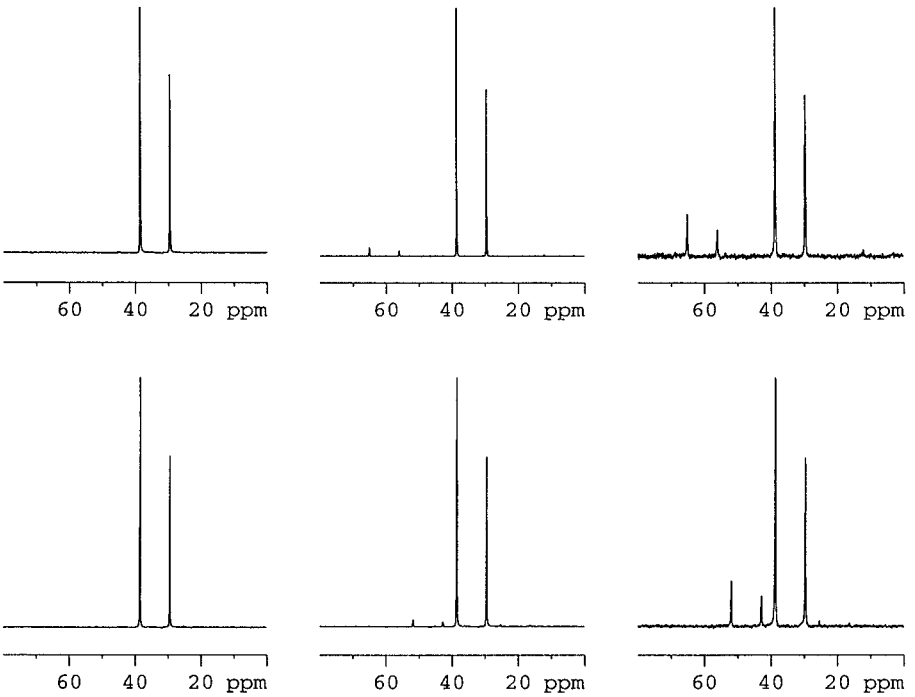

FIG. 3. Comparison of the radial-field sideband intensities in the standard ^{13}C CP/MAS spectra of adamantane recorded at spinning frequencies of 1 (bottom) and 2 kHz (top) for a (left) 3-mm slice of sample placed in the central part of the rotor; (middle) whole rotor; (right) 3-mm slice of sample placed at the bottom of the rotor. A standard 7-mm CP/MAS Bruker probe has been used (for technical details see Fig. 2). Each spectrum is presented with the same full intensity of the isotropic CH_2 signal (the intensity of -1 radial-field induced sidebands for middle and the right-hand spectra is, respectively, 3 and 17% of the central peaks).

modulated chemical shift anisotropy of benzene molecules but is completely ineffective in suppression of the purely radial-field sidebands of C_{60} which now appear with arbitrary phases. The radial-field effect may also be the reason for the presence of the residual -1 sideband of benzene in the TOSS spectrum.

CONCLUSIONS

This paper describes theoretically and illustrates experimentally a contribution to sidebands intensities in solid-state MAS spectra arising from magnetization excited by the radial com-

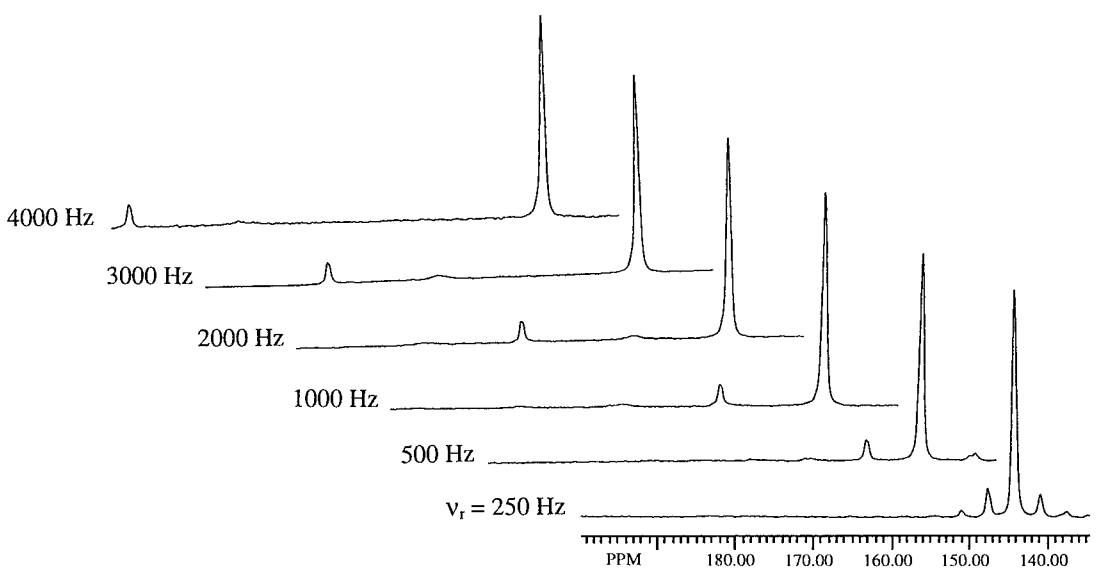

FIG. 4. Effect of the "purely radial-field" -1 sideband of C_{60} signal in the one-pulse ^{13}C spectra of benzene-solvated C_{60} for a small volume sample placed at the edge of coil and recorded at different spinning frequencies.

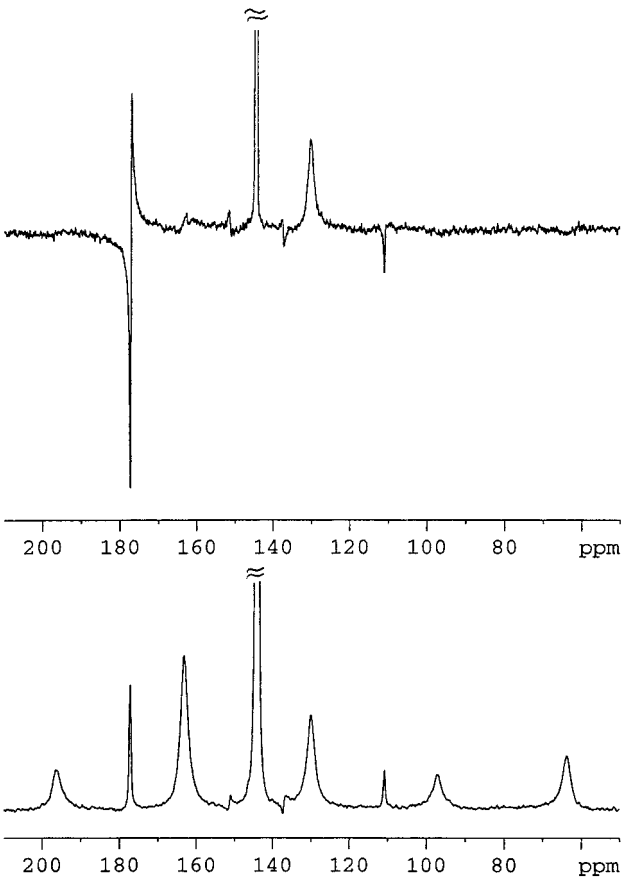

FIG. 5. ^{13}C CP/MAS spectra of benzene-solvated C_{60} for a small volume sample placed at the edge of coil and recorded at spinning frequency of 2.5 kHz without (bottom) and with (top) suppression of CSA spinning sidebands by the TOSS method. In this compound the anisotropic rotation dominates the motion of benzene molecules leading to a pronounced chemical shift anisotropy at room temperature (*10*). For the purpose of comparison, both spectra have been shown with the same height of the isotropic peak of benzene at 128.5 ppm.

ponent of the RF field at the edges of the coil. We have shown that, for a sample placed in a rotor of length exceeding the solenoid coil or for a small volume sample placed at the edge of the coil, the radial-field effect may contribute significantly to the intensity of the -1 spinning sideband of rotor-modulated internal interaction. This may lead to errors in the analysis of ssb manifolds when extracting the structural and motional information through the principal values of corresponding tensors and their mutual orientations. The radial-field sidebands may also manifest themselves when using the techniques of suppression of spinning sidebands. In general, the effect of radial-field sidebands will be attenuated in the rare spin spectra requiring a high-power proton decoupling due to the broadening of the resonance signals under lower RF decoupling field at the edges of the coil. As demonstrated above, things would be different in the presence of small dipolar interactions encountered in highly mobile or magnetically dilute systems as well as in most inorganic solids.

ACKNOWLEDGMENTS

We thank Dr. F. Masin for providing the sample of benzene-solvated C_{60} and Dr. M. Potrzebowski for preliminary experimental verifications.

REFERENCES

1. M. Goldman, V. Fleury, and M. Guéron, NMR frequency shift under sample spinning, *J. Magn. Reson. A* **118,** 11–20 (1996).
2. R. G. Griffin, Spinning sidebands, *in* "Encyclopedia of Magnetic Resonance" (D. M. Grant, Ed.), pp. 4174–4185, Wiley, New York, 1996.
3. D. I. Hoult and R. E. Richards, The signal-to-noise ratio of the nuclear magnetic resonance experiment, *J. Magn. Reson.* **24,** 71–85 (1976).
4. E. K. Insko, M. A. Elliott, J. C. Schotland, and J. S. Leigh, General reciprocity, *J. Magn. Reson.* **131,** 111–117 (1998).
5. R. Freeman, Sample spinning, *in* "A Handbook of Nuclear Magnetic Resonance," p. 194, Longman Scientific & Technical, Harlow, England, 1998.
6. E. R. Malinowski and A. R. Pierpaoli, Asymmetric spinning sidebands from coaxial cells in NMR spectra, *J. Magn. Reson.* **1,** 509–515 (1969).
7. M. Vera and J. B. Grutzner, The Taylor vortex: The measurement of viscosity in NMR samples, *J. Am. Chem. Soc.* **108,** 1304–1305 (1986).
8. J. Taquin, Signal de précession libre et bandes latérales de rotation en RMN de haute résolution par transformée de Fourier en présence de champs magnétiques inhomogènes, *C. R. Acad. Sci. Paris* **284,** B145–B148 (1977).
9. M. H. Levitt, T. G. Oas, and R. G. Griffin, Rotary resonance recoupling in heteronuclear spin pair systems, *Isr. J. Chem.* **28,** 271–282 (1988).
10. P. Tekely, P. Palmas, P. Mutzenhardt, F. Masin, A. S. Grell, I. Messari, and M. Gelbcke, Structural and motional features of benzene-solvated C_{60} as revealed by high-resolution solid state NMR, *Solid State Commun.* **106,** 391–395 (1998).